Bioconjugate Chemistry

Communication

pubs.acs.org/bc

Fine-Tuned H-Ferritin Nanocage with Multiple Gold Clusters as Near-Infrared Kidney Specific Targeting Nanoprobe

Cuiji Sun,[†] Yi Yuan,[†,§] Zhonghe Xu,[⊥] Tianjiao Ji,[†] Yanhua Tian,[†] Shan Wu,[§] Jianlin Lei,[§] Jingyuan Li,*[,⊥] Ning Gao,*[,§] and Guangjun Nie*[,†]

[†]CAS Key Laboratory for Biomedical Effects of Nanomaterials & Nanosafety, National Center for Nanoscience and Technology, 100190 Beijing, China

[§]MOE Key Laboratory of Protein Sciences, Center for Structural Biology, School of Life Sciences, Tsinghua University, 100084 Beijing, China

[⊥]CAS Key Laboratory for Biomedical Effects of Nanomaterials and Nanosafety, Institute of High Energy Physics, Chinese Academy of Sciences, 100049 Beijing, China

S *Supporting Information*

ABSTRACT: When stabilized and functionalized by biomolecules, noble metal (such as gold and silver) cluster-based hybrid nanocomposites have shown great promise for biomedical applications, due to their unique physiochemical properties originating from the inorganic elements and specific functionality and biocompatibility from their biological components. Although certain promise for bioimaging, biosensing, and biomimetic catalysis has been demonstrated, it is still a great challenge to integrate the defined functionality of the biomolecules with enhanced or novel physiochemical properties of the metal clusters, under control at the molecular level. Herein, based on molecular dynamics simulation of a gold (Au) cluster assembly, we designed near-infrared (NIR) fluorescent hybrid nanocomposites with multiple Au clusters within an apo H-ferritin (HFt) nanocage. The fluorescence quantum yield of near-infrared (NIR) Au-HFt is about 63.4% and the emission peak is 810 nm. The NIR Au-HFt is one of the first native protein-guided Au cluster-based nanomaterials for in vivo biowindow imaging. In vivo fluorescent imaging and quantification of Au element confirmed that Au-HFt not only retained the kidney targeting properties of HFt well (about 10 times higher Au concentration in kidney than in liver and spleen, the most common organs for nanoparticle accumulation), but also gained strong NIR imaging capability for live animals. The NIR Au-HFt showed powerful tissue penetrating ability, strong fluorescent efficiency, and excellent kidney targeting specificity. These results thus open new opportunities for kidney disease imaging and theranostic applications.

Bioinorganic hybrid nanomaterials have attracted wide attention for a variety of biomedical applications, such as bioimaging,[1−3] biosensing,[4−6] drug delivery,[7,8] and biomimetic catalysis,[9−11] due to their integrated properties from both the biomolecules for specific functionality and biocompatibility and the inorganic components for desired physiochemical properties, such as optimized optical properties.[1−3] Gold (Au) clusters, which possess certain molecular and atomic properties, have shown great promise for biomedical applications, due to their size-dependent intrinsic photoluminescence, specific catalytic activities, high stability, and low cytotoxicity.[1,3,4,12−15] The integration of Au clusters with biomolecules, especially proteins, has created many novel nanocomposites in recent years, and the superior catalytic and photonic properties of Au clusters have been demonstrated.[1,3,4,12,15] By controlling the specific binding of Au ion to scaffold proteins, and the growth of Au clusters within scaffold proteins, these clusters have been assembled into various protein structures, such as bovine serum albumin (BSA), ferritin, and trypsin, to form novel biomimetic molecules with various desired photoluminescent properties for bioimaging applications.[1,3,4,16,17] However, due to the weak tissue penetration of the fluorescent probes within the UV−vis range, low fluorescence quantum yields, relatively weak fluorescence intensity, and lack of targeting specificity,[18,19] their applications in live animal imaging and theranostic applications are largely limited. As a result, development of next-generation near-infrared (NIR) nanoprobes with high tissue specificity, fluorescence quantum yield and penetration, as well as defined cellular binding and uptake specificity, is urgently needed. In this context, we first carried out molecular dynamics (MD) simulation to study the formation and growth of Au clusters within a ferritin nanocage. We then developed a straightforward method to integrate multiple NIR fluorescent Au clusters within an apo H-ferritin (HFt) nanocage for in vivo

Received: November 17, 2014
Revised: January 15, 2015
Published: January 16, 2015

DOI: 10.1021/bc5005284
Bioconjugate Chem. 2015, 26, 193−196

fluorescent imaging and receptor-mediated kidney-specific targeting.

Ferritins, composed of 24 subunits of different ratios of H- and L-ferritin subunits (HFt and LFt), are a type of symmetric protein nanocage[20,21] that have been investigated extensively. HFt, but not LFt, has a ferroxidase enzymatic center responsible for incorporation of metal iron under physiological conditions.[20,21] Specific binding proteins for both HFt and LFt have been reported and characterized in animal and human cells.[22,23] In our previous work, we have successfully synthesized Au-Ft from horse spleen ferritin (22 LFt and 2 HFt), which contained a pair of Au clusters formed in the ferritin nanocage.[1] We showed the potential of this type of Au-Ft in far-red fluorescent imaging of kidney in live animals, due to the specific L-ferritin binding protein Scara 5 expressed in kidney cells.[1,22] To further elucidate the Au cluster nucleation and growth mechanism, enhance the imaging capability, and optimize fluorescent emission to the infrared range for better tissue penetration via controlling the growth and interaction of Au clusters, we chose to work with recombinant human HFt (composed of 24 HFt subunits). In principle, ferritin nanocages made of solely HFt would contain more ferroxidase centers and allow growth of even more Au clusters within the nanocage. In addition, HFt also has a specific high affinity receptor Tim-2, which is expressed in renal tubule cells,[23,24] and thus could retain its high specificity to kidney.[23,24] Recombinant human HFt also adopts a rhombic dodecahedral structure with two subunits (dimer) on each rhombic face. Each HFt subunit has a ferroxidase center and a nucleation center for iron ion and both sites are on the inner surface of an HFt subunit and close to each other. Importantly, there are three histidine (His) residues distributed in these sites[20,21] (His65 in ferroxidase center and His57, His60 in nucleation center; Supporting Information Figure S1). It has been well demonstrated that Au atoms can be attracted to His residues because of their interaction with imidazole rings of His residues.[25,26] In addition, His residues of two adjacent HFt subunits on the same rhombic face are close to each other, especially His57 and His60 in the nucleation centers of the two subunits (Supporting Information Figure S1). Taken together, there is a putative Au deposition region in each dimer, and each region is composed of around six His residues.

We then investigated the growth of Au clusters on the putative Au deposition region of subunit dimers and performed an in silica analysis (Figure 1). Specifically, a fragment of HFt nanocage, which is composed of six HFt subunits (three dimers), was subjected to MD simulation to study the formation and growth of Au clusters therein (Supporting Information Figure S2).[27,28] As shown in Figure 1a, Au atoms were preferentially adsorbed on the putative Au deposition region composed of His residues of two HFt subunits. After 320 ns simulation, Au clusters formed on the inner surface of all three dimers. Hence, there could be up to 12 Au clusters in a complete Au-HFt (Figure 1b). For clarification, Figure 1c shows Au clusters on subunit octadecamer after removing the hexamer in the upper part of HFt, and the number of Au atoms in a single cluster can be up to 87 (Figure 1a) under saturated Au ion concentration. The distance between adjacent Au clusters is around 33 Å (Figure 1d).

The results of MD simulation confirmed our hypothesis that more Au clusters with larger size and more red-shifted fluorescence emission properties can be realized when introducing 24mers of HFt (up to 12 clusters, each with

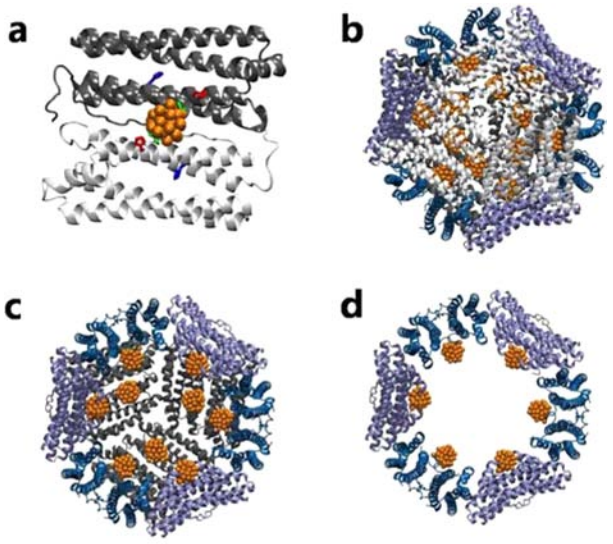

Figure 1. Model of multiple Au cluster-containing HFt. (a) Au clusters adsorbed on the internal surface of subunit dimer (t = 320 ns); (b) Au clusters within a complete HFt nanocage; (c) Au clusters on subunit octadecamer (removing the hexamer in the upper part of HFt); (d) Au clusters on the dodecamer distributed at the equator of HFt. The subunits in the upper part and lower part of HFt are in light and dark gray, respectively, and the subunits at the equator of HFt are colored purple and navy alternatively.

around 87 Au atoms). Then, we tried to optimize the assembly process of the Au-HFt in vitro and analyzed its optical properties. Figure 2a showed that its excitation peak is about 722 nm and the emission peak can move to about 810 nm under saturated Au concentration and optimized growth condition. The fluorescence quantum yield of NIR Au-HFt is 63.4%, much higher than that of all the Au cluster related nanomaterials before.[1,3,4,29] Since NIR has good tissue

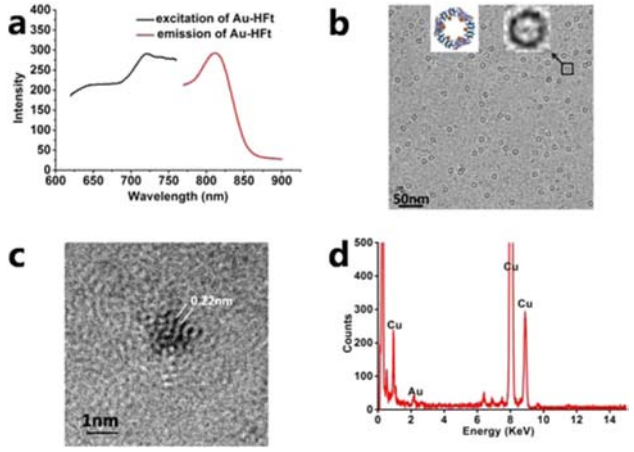

Figure 2. Characteristics of Au-HFt with multiple Au clusters. (a) NIR fluorescent excitation and emission spectra of Au-HFt. (b) Cryo-EM image of the Au-HFt particles in native state. Three pairs of Au clusters were observed within the HFt nanocage, and MD stimulation suggests six Au clusters on the dodecamer, which distribute at the equator of ferritin (indicated by square and arrow in the inset). (c) HRTEM imaging of air-dried Au-HFt showing Au clusters at higher resolution. The crystal lattice spacing is about 0.22 nm (inset) and the 111 face of Au is evident. (d) EDS of NIR Au-HFt showing the presence of elemental Au.

DOI: 10.1021/bc5005284
Bioconjugate Chem. 2015, 26, 193−196

penetrating ability,[16,17] and high quantum yield of NIR Au-HFt, the NIR Au-HFt should be well suited for in vivo biomedical imaging with intact samples.

To confirm the MD simulation-based prediction of the number of Au clusters within a single Au-HFt, we used cryo-electron microscopy (cryo-EM) to measure Au clusters in HFt. In Figure 2b and Supporting Information Figure S3, we observed about 6 Au clusters distributed in the edge region of HFt. The edge region observed in cryo-EM images corresponds to the equatorial plane of HFt. According to its dodecahedral structure, around six dimers distribute in the equatorial plane, and the other six dimers distributed in the remaining part of hemispheres (Figure 2b). The result of cryo-EM imaging suggests there is one Au cluster in each dimer, in agreement with the prediction of the MD simulation. In Figure 2c, high resolution transmission electron microscopy (HRTEM) imaging also shows that the crystal lattice spacing is about 0.22 nm (inset) and the 111 face of Au is evident. Additional, energy-dispersive-X-ray spectroscopy (EDX) experiments confirmed the presence of elemental Au, but not iron, in the Au-HFt samples (Figure 2d).

After characterizing the NIR property of Au-HFt, we applied this hybrid material for live animal imaging in nude mice. As shown in Figure 3a, strong NIR fluorescent spectra of kidney-

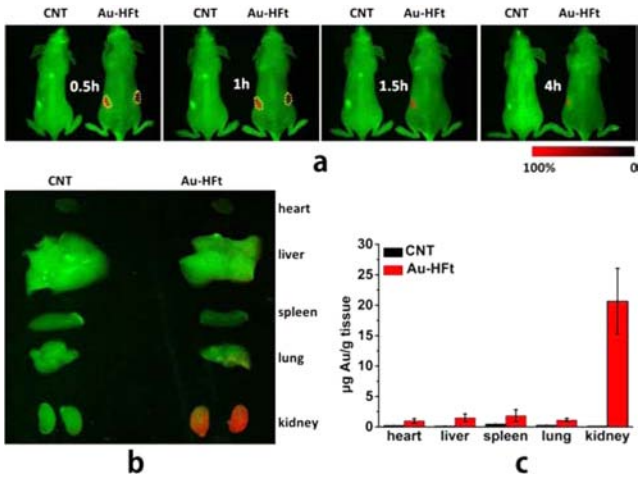

Figure 3. In vivo and ex vivo NIR fluorescent imaging and ICP-MS analyses show the specificity of Au-HFt to kidneys in nude mice. (a) Whole body NIR fluorescence images of nu/nu female mice at different time points after Au-HFt injection into the tail vein. The final concentration of Au-HFt was 0.2 nmol/g body weight. For each panel, the Au-HFt injected mouse is shown on the right and a saline injected control (CNT) is shown on the left. (b) NIR fluorescence images of nu/nu female mouse organs 1 h after Au-Ft tail vein injection (red color represents NIR fluorescence of Au-HFt and green color represents background). (c) ICP-MS analysis shows the specific tissue accumulation of Au, the distribution of Au in various tissues 1 h after injection of Au-HFt.

like structures (red color) can be detected in the dorsal view 0.5 h after injection of Au-HFt, but not in other organs of the nude mice. In contrast, there are no NIR fluorescent signals in the kidneys of the nude mice injected with saline. Consistently, in the ex vivo imaging of organs from the experimental and control mice, strong NIR fluorescent spectra are only detected in the kidneys (red color) of Au-HFt injected mice, but not other organs. To confirm these results, we used inductively coupled plasma mass spectrometry (ICP-MS) to quantitatively show Au distribution and tissue specific accumulation in various tissues at 1 h after injection of Au-HFt and saline. The results of ICP-MS are highly consistent with the live fluorescent imaging. More than ten times higher concentration of Au element accumulated in the kidney than the other common major organs (such as liver and spleen, the most common organs for nanoparticle accumulation) were observed. Therefore, both the fluorescent imaging and ICP-MS results demonstrate that NIR Au-HFt has a strong fluorescent penetrating ability and a sole kidney targeting specificity.

In this work, we designed apo H-ferritin to incubate multiple NIR fluorescent Au clusters in the cavity of human HFt and demonstrated its exceptional kidney targeting and whole body imaging abilities. To our knowledge, this is the first study of NIR fluorescent Au clusters within native proteins. This hybrid material has two advantages. First, its emission fluorescent spectrum is NIR and it has high fluorescence quantum yield, which enables a better fluorescent penetrating property than common/conventional Au clusters. Second, it has solo-kidney targeting ability, which is, according to the best of our knowledge, one of the highest kidney-specific hybrid nanocomposites among all engineered nanoparticles. In summary, we provide a general route for the controlled assembly of noble metal clusters within low toxicity and bioactive nanostructures. In addition, Au-HFt with high stability in physiological conditions provides a basis for future large-scale practical application. The combination of these desired properties might pave the way for synthesis of various novel bionanostructures for biomedical applications.

■ ASSOCIATED CONTENT

Supporting Information

Experimental details, synthetic procedures, characterization methods, molecular dynamics simulations, and additional figures. This material is available free of charge via the Internet at http://pubs.acs.org.

■ AUTHOR INFORMATION

Corresponding Authors

*E-mail: niegj@nanoctr.cn.
*E-mail: ninggao@tsinghua.edu.cn.
*E-mail: lijingyuan@ihep.ac.cn.

Author Contributions

Cuiji Sun and Yi Yuan contributed equally.

Notes

The authors declare no competing financial interest.

■ ACKNOWLEDGMENTS

This work was supported by the grants from National Basic Research Plan of China (MoST 973 Program 2012CB934004 and 2013CB933704), the National Distinguished Youth Scientists program (31325010) of NSFC, and Beijing Higher Education Young Elite Teacher Project (YETP0131).

■ REFERENCES

(1) Sun, C., Yang, H., Yuan, Y., Tian, X., Wang, L., Guo, Y., Xu, L., Lei, J., Gao, N., and Anderson, G. J. (2011) Controlling assembly of paired gold clusters within apoferritin nanoreactor for in vivo kidney targeting and biomedical imaging. *J. Am. Chem. Soc. 133*, 8617−8624.
(2) Chan, Y. H., Ye, F., Gallina, M. E., Zhang, X., Jin, Y., Wu, I. C., and Chiu, D. T. (2012) Hybrid semiconducting polymer dot-quantum dot with narrow-band emission, near-infrared fluorescence, and high brightness. *J. Am. Chem. Soc. 134*, 7309−7312.

DOI: 10.1021/bc5005284
Bioconjugate Chem. 2015, 26, 193−196

(3) Xie, J., Zheng, Y., and Ying, J. Y. (2009) Protein-directed synthesis of highly fluorescent gold nanoclusters. *J. Am. Chem. Soc. 131*, 888−889.
(4) Liu, J.-M., Chen, J.-T., and Yan, X.-P. (2013) Near infrared fluorescent trypsin stabilized gold nanoclusters as surface plasmon enhanced energy transfer biosensor and in vivo cancer imaging bioprobe. *Anal. Chem. 85*, 3238−3245.
(5) Chen, Y. S., Choi, H., and Kamat, P. V. (2013) Metal-cluster-sensitized solar cells. A new class of thiolated gold sensitizers delivering efficiency greater than 2%. *J. Am. Chem. Soc. 135*, 8822−8825.
(6) Sahoo, S., Husale, S., Karna, S., Nayak, S. K., and Ajayan, P. M. (2011) Controlled assembly of Ag nanoparticles and carbon nanotube hybrid structures for biosensing. *J. Am. Chem. Soc. 133*, 4005−4009.
(7) Sanchez, C., Belleville, P., Popall, M., and Nicole, L. (2011) Applications of advanced hybrid organic−inorganic nanomaterials: from laboratory to market. *Chem. Soc. Rev. 40*, 696−753.
(8) Gibson, J. D., Khanal, B. P., and Zubarev, E. R. (2007) Paclitaxel-functionalized gold nanoparticles. *J. Am. Chem. Soc. 129*, 11653−11661.
(9) Moisan, S., Martinez, V., Weisbecker, P., Cansell, F., Mecking, S., and Aymonier, C. (2007) General approach for the synthesis of organic-inorganic hybrid nanoparticles mediated by supercritical CO_2. *J. Am. Chem. Soc. 129*, 10602−10606.
(10) Woolerton, T. W., Sheard, S., Reisner, E., Pierce, E., Ragsdale, S. W., and Armstrong, F. A. (2010) Efficient and clean photoreduction of CO_2 to CO by enzyme-modified TiO_2 nanoparticles using visible light. *J. Am. Chem. Soc. 132*, 2132−2133.
(11) Hong, R., Emrick, T., and Rotello, V. M. (2004) Monolayer-controlled substrate selectivity using noncovalent enzyme-nanoparticle conjugates. *J. Am. Chem. Soc. 126*, 13572−13573.
(12) Chen, T., Hu, Y., Cen, Y., Chu, X., and Lu, Y. (2013) A dual-emission fluorescent nanocomplex of gold-cluster-decorated silica particles for live cell imaging of highly reactive oxygen species. *J. Am. Chem. Soc. 135*, 11595−11602.
(13) Turner, M., Golovko, V. B., Vaughan, O. P., Abdulkin, P., Berenguer-Murcia, A., Tikhov, M. S., Johnson, B. F., and Lambert, R. M. (2008) Selective oxidation with dioxygen by gold nanoparticle catalysts derived from 55-atom clusters. *Nature 454*, 981−983.
(14) Zhang, J., Sasaki, K., Sutter, E., and Adzic, R. (2007) Stabilization of platinum oxygen-reduction electrocatalysts using gold clusters. *Science 315*, 220−222.
(15) Palmer, R., Pratontep, S., and Boyen, H.-G. (2003) Nano-structured surfaces from size-selected clusters. *Nat. Mater. 2*, 443−448.
(16) Becker, A., Hessenius, C., Licha, K., Ebert, B., Sukowski, U., Semmler, W., Wiedenmann, B., and Grötzinger, C. (2001) Receptor-targeted optical imaging of tumors with near-infrared fluorescent ligands. *Nat. Biotechnol. 19*, 327−331.
(17) Weissleder, R., Tung, C.-H., Mahmood, U., and Bogdanov, A. (1999) In vivo imaging of tumors with protease-activated near-infrared fluorescent probes. *Nat. Biotechnol. 17*, 375−378.
(18) Rudin, M., and Weissleder, R. (2003) Molecular imaging in drug discovery and development. *Nat. Rev. Drug Discovery 2*, 123−131.
(19) Weissleder, R. (2002) Scaling down imaging: molecular mapping of cancer in mice. *Nat. Rev. Cancer 2*, 11−18.
(20) Chasteen, N. D., and Harrison, P. M. (1999) Mineralization in ferritin: an efficient means of iron storage. *J. Struct. Biol. 126*, 182−194.
(21) Levi, S., Yewdall, S. J., Harrison, P. M., Santambrogio, P., Cozzi, A., Rovida, E., Albertini, A., and Arosio, P. (1992) Evidence of H- and L-chains have co-operative roles in the iron-uptake mechanism of human ferritin. *Biochem. J. 288*, 591−596.
(22) Li, J. Y., Paragas, N., Ned, R. M., Qiu, A., Viltard, M., Leete, T., Drexler, I. R., Chen, X., Sanna-Cherchi, S., and Mohammed, F. (2009) Scara5 is a ferritin receptor mediating non-transferrin iron delivery. *Dev. Cell 16*, 35−46.
(23) Chen, T. T., Li, L., Chung, D.-H., Allen, C. D., Torti, S. V., Torti, F. M., Cyster, J. G., Chen, C.-Y., Brodsky, F. M., and Niemi, E. C. (2005) TIM-2 is expressed on B cells and in liver and kidney and is a receptor for H-ferritin endocytosis. *J. Exp. Med. 202*, 955−965.
(24) Han, J., Seaman, W. E., Di, X., Wang, W., Willingham, M., Torti, F. M., and Torti, S. V. (2011) Iron uptake mediated by binding of H-ferritin to the TIM-2 receptor in mouse cells. *PLoS One 6*, e23800.
(25) Herrero, M. A., Guerra, J., Myers, V. S., Gomez, M. V., Crooks, R. M., and Prato, M. (2010) Gold dendrimer encapsulated nanoparticles as labeling agents for multiwalled carbon nanotubes. *ACS Nano 4*, 905−912.
(26) Knecht, M. R., Garcia-Martinez, J. C., and Crooks, R. M. (2005) Hydrophobic dendrimers as templates for Au nanoparticles. *Langmur 21*, 11981−11986.
(27) Lawson, D. M., Artymiuk, P. J., Yewdall, S. J., Smith, J. M., Livingstone, J. C., Treffry, A., Luzzago, A., Levi, S., Arosio, P., and Cesareni, G. (1991) Solving the structure of human H ferritin by genetically engineering intermolecular crystal contacts. *Nature 349*, 541−544.
(28) Oostenbrink, C., Villa, A., Mark, A. E., and Van Gunsteren, W. F. (2004) A biomolecular force field based on the free enthalpy of hydration and solvation: The GROMOS force-field parameter sets 53A5 and 53A6. *J. Comput. Chem. 25*, 1656−1676.
(29) Zheng, J., Nicovich, P. R., and Dickson, R. M. (2007) Highly fluorescent noble metal quantum dots. *Annu. Rev. Phys. Chem. 58*, 409.

DOI: 10.1021/bc5005284
Bioconjugate Chem. 2015, 26, 193−196